Spin control and manipulation in (111) GaAs quantum wells

A. Hernández-Mínguez*[a], K. Biermann[a], R. Hey[a], P. V. Santos[a]
[a]Paul-Drude-Institut für Festkörperelektronik, Hausvogteiplatz 5-7, 10117 Berlin, Germany

ABSTRACT

The control of spin dephasing is an essential requirement for quantum information processing using electron spins in III-V semiconductors. GaAs quantum wells grown along the non-conventional [111] crystallographic direction are particularly interesting for spintronics due to the long spin lifetimes, which can be electrically controlled. Here, we show electron spin dynamics in (111) quantum wells by combining spatially-resolved with time-resolved photoluminescence measurements. The latter allows us to experimentally demonstrate the field induced enhancement of the spin lifetime as well as the transport of spin over several micrometers along the quantum well plane.

Keywords: spin, GaAs, spin-orbit coupling, photoluminescence

1. INTRODUCTION

The manipulation of spins in semiconductor materials has become an active area of investigation, in particular after different proposals for spin-based electronic information processing have been put forward. Device functionalities based on electron spins require processes for the generation, storage, detection, and transport of spins as well as interaction mechanisms to manipulate the spin vector. In this respect, the spin coherence time in intrinsic III-V bulk semiconductors is typically on the order of only one ns, thus restricting the number of spin manipulation steps that can be realized before decoherence effects set in. Therefore, the two main challenges for an efficient manipulation of the spin vector are (i) the enhancement of the electron spin coherence times, and (ii) the development of spin manipulation techniques that do not compromise the spin lifetime.

While isolated spins can be efficiently manipulated using a magnetic field, electron spins in a crystal interact with other spins from electrons (the exchange interaction) or nuclei (the hyperfine interaction) as well as with the lattice potential. These interactions can be used for the realization of spin control gates, but also lead to spin relaxation if not appropriately controlled. The electron-hole exchange interaction leads to the so-called Bir-Aronov-Pikus (BAP) spin dephasing mechanism, which is particularly important for excitons as well as in highly p-type doped III-V semiconductors at low temperatures. Spin scattering via the hyperfine-interaction is normally negligible for free carriers, but becomes important for localized electrons in quantum dots.

Electron spins in semiconductors are also affected by the orbital motion and the lattice potential via the spin-orbit (SO) interaction. This interaction arises from the fact that an electron moving through a non-centrosymmetric crystal (such as the zinc-blende semiconductors) experiences a varying electric field. In the electron reference frame, the latter translates into a momentum ($\hbar\mathbf{k}$) dependent effective magnetic field, $\mathbf{B}_{SO}(\mathbf{k})$, which acts on its spin, as illustrated in Figure 1(a). As the SO-interaction can be controlled by external electric and strain fields, it provides an interesting mechanism for spin manipulation without the application of external magnetic fields. Examples are the generation of non-equilibrium spin populations using electric currents, as well as the spin galvanic and spin Hall effects.

The SO-interaction, however, can also lead to spin dephasing in an electron ensemble. Since $\mathbf{B}_{SO}$ depends on $\mathbf{k}$, the SO-field experienced by a moving electron will change its strength and direction after each electron scattering event. As a result, each electron spin within an ensemble will precess around a different axis and at a different rate in between two consecutive scattering events, leading to a reduction of the initial spin polarization of the spin ensemble. This effect is known as Dyakonov-Perel (DP) spin dephasing. The SO-interaction can also couple different spin states during electron scattering processes. One example is the Elliott-Yafet spin dephasing mechanism, which describes spin-flip transitions induced during electron scattering by impurities or phonons and is expected to be influential in highly doped, low-bandgap materials. Finally, the SO-coupling also accounts for the intersubband spin relaxation mechanism in QW structures, in which electron scattering between two subbands is accompanied by a spin flip.

In this contribution, we investigate the electric control of spins in III-V semiconductor quantum wells (QWs) grown along the non-conventional [111] crystallographic direction. The studies were motivated by the special characteristics of the SO-interaction in these structures, which is discussed in Sec. 2. After a description of the experimental procedures to optically generate and probe spins (Sec. 3), we present experimental results demonstrating that an electric field can efficiently control the SO-interaction in GaAs(111) QWs. In particular, a strong suppression of the spin dephasing mechanisms related to the SO can be achieved, leading to very long spin lifetimes (~ 50 ns). Furthermore, the long living spins can be transported over microscopic distances (> 10 μm) along the QW plane. To our knowledge, this results show the first demonstration of spin transport in (111) structures. The mechanisms for the enhanced lifetimes and transport distances are then discussed in Sec. 4, while Sec. 5 summarizes the main conclusions of this work.

2. SYMMETRY OF THE SPIN-ORBIT INTERACTION IN III-V QUANTUM WELLS

The SO-interaction in III-V QWs is governed by two major contributions. The first is of intrinsic nature and associated with the bulk inversion asymmetry (BIA) of the III-V zinc-blende lattice. The amplitude and orientation of the effective SO-magnetic field associated with this contribution, which is normally denoted as the Dresselhaus field ($\mathbf{B_D}$), depends on the crystallographic growth orientation of the QW. The wave vector dependences of $\mathbf{B_D}$ for (001) and (111) QWs are compared in Fig. 1(c). These results are valid in the region of small $\mathbf{k}$ ($k<<\pi/d_{QW}$, where d_{QW} denotes the QW thickness) where the amplitude of $\mathbf{B_D}$ becomes proportional to $\mathbf{k}$. In both cases, $\mathbf{B_D}$ lies in the QW plane. Note, however, that while $\mathbf{B_D}$ in (001) QWs follows a relatively complex angular dependence, it is always perpendicular to $\mathbf{k}$ in (111) structures.

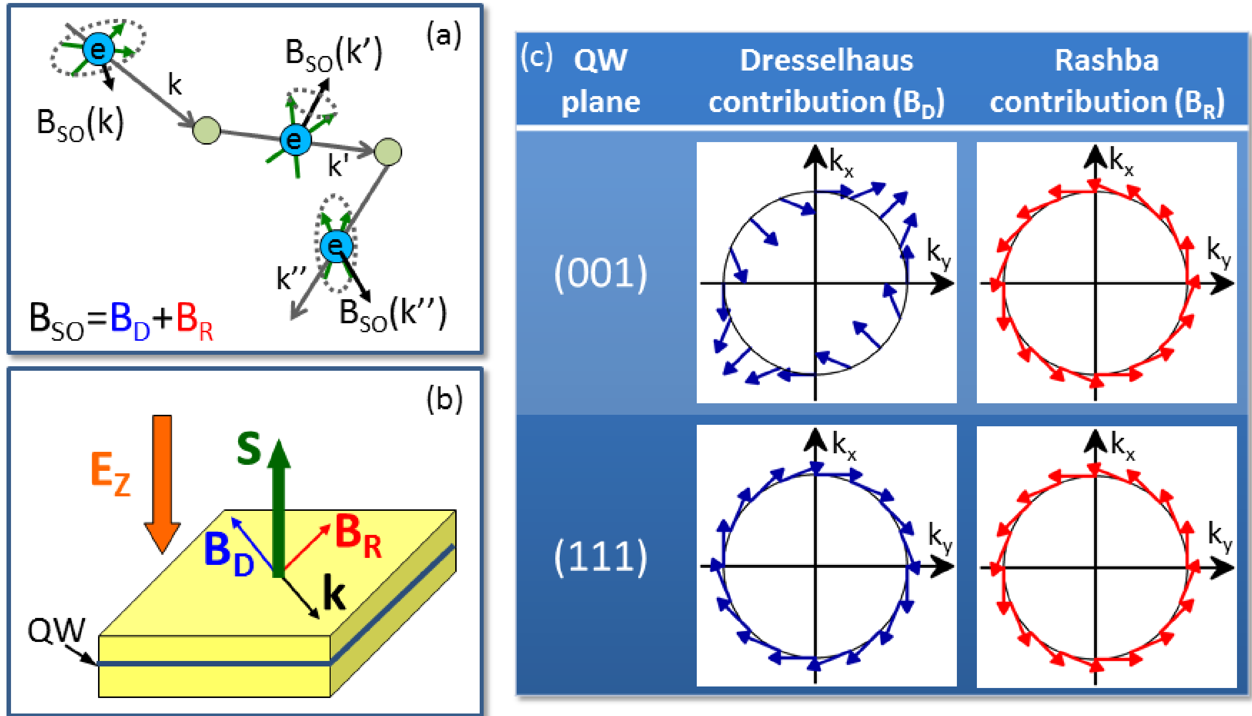

Figure 1. (a) Spin dephasing associated with the SO-interaction. During motion, a spin rotates around an effective magnetic field, $\mathbf{B_{SO}}$, whose amplitude and direction depend on the electron wave vector, $\mathbf{k}$. (b) Relative orientation of the Dresselhaus ($\mathbf{B_D}$) and Rashba ($\mathbf{B_R}$) contributions to the SO-field acting on an electron spin ($\mathbf{S}$) oriented perpendicular to the quantum well (QW) plane. The Rashba field is induced by an electric field (E_Z) applied perpendicularly to the QW plane. (c) Symmetry of the Dresselhaus and Rashba SO-fields in GaAs (001) and (111) quantum wells. In the reference frame used by us, x = [110] and y = [-110] for (001) QWs, while x = [-1-12] and y = [1-10] for (111) QWs [1].

The second important contribution to the SO-interaction arises from structural inversion asymmetries (SIA) in the QW potential introduced by external fields. In most cases, the SIA is generated by an electric field (E_Z) applied perpendicularly to the QW plane (cf. Fig. 1(b)), leading to the so-called Rashba SO-field ($\mathbf{B_R}$). The latter always lies in the QW plane with

an orientation perpendicular to **k** (cf. Fig. 1(c)). Since its strength depends on E_Z, the Rashba field provides a powerful tool for the electric manipulation of the spin vector.

The Dresselhaus and Rashba fields in Fig. 1(c) become collinear for particular values of **k**. Under these certain circumstances, the tunable Rashba field can be used to compensate the Dresselhaus contribution, thereby suppressing the total SO-field for these **k**'s. In the case of (001) QWs, this occurs for **k** along a <110> orientation. This property has been explored to create long living spin helix states [2, 3].

(111) QWs are particular interesting for SO suppression because the linear terms in **k** of the Rashba and Dresselhaus contributions have exactly the same symmetry (cf. Fig. 1(c)). As a result, if one adjusts the electric field to satisfy the condition: $\mathbf{B_R}(\mathbf{k}) + \mathbf{B_D}(\mathbf{k}) = 0$, the total SO-field will vanish simultaneously for all orientations of **k**. The electric field E_C required of compensation is given approximately by [1, 4]:

$$E_C = \frac{\gamma}{\sqrt{3}r_{41}}\left[\left(\frac{\pi}{d_{eff}}\right)^2 - \frac{1}{4}\langle k_\parallel^2\rangle\right] \qquad (1)$$

Here, γ and r_{41} are the Rashba and Dresselhaus coefficients, respectively, $\langle k_\parallel^2\rangle$ is the thermal average of the squared component of **k** parallel to the QW plane, and d_{eff} is the effective extension of the electronic wave function along the growth direction, which depends on the QW thickness and on the penetration length on the barrier layers. Equation 1 is valid for $k \ll \pi/d_{eff}$. Provided that the electron ensemble populates states with small *k*-vectors, such as in intrinsic QWs at low temperatures, the $k_\parallel$ contribution can be neglected and the total field $\mathbf{B_{SO}}$ vanishes for all **k**'s independently of their amplitude and orientation. This compensation mechanism was originally proposed in the theoretical works by Cartoixà [5] and Vurgaftman [6]. Evidence for the enhancement of the spin lifetime with bias was provided by the works by Ballocchi *et al.* [7], and Biermann *et al.* [8]. Finally, Hernández-Mínguez *et al.* [4] have provided the experimental verification of the BIA/SIA compensation mechanism by demonstrating the electrically driven transition from a Dresselhaus-dominated spin dephasing regime to a Rashba-dominated one with increasing electric field.

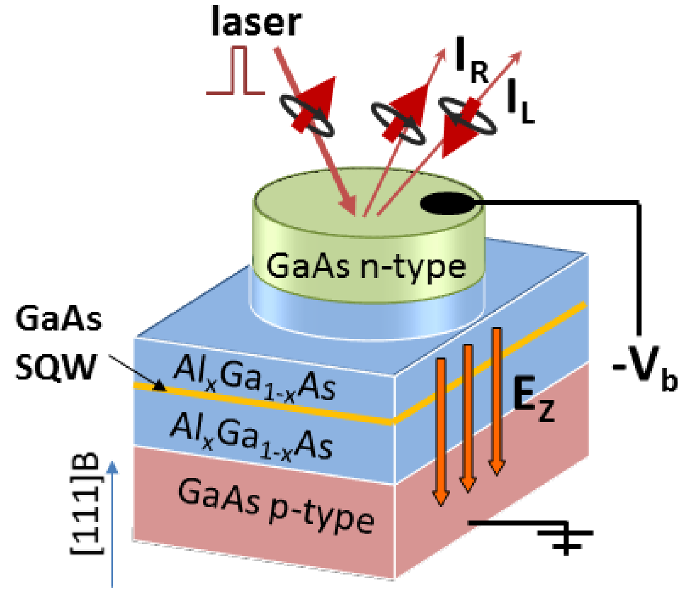

Figure 2. Structure of a single quantum well (SQW) embedded within a n-i-p diode structure grown along the [111]B direction of a GaAs substrate. Spin polarized electron-hole pairs are optically excited by a pulsed laser beam focused on a small spot on the sample surface. The electric field E_Z induced by the bias V_b applied between the semitransparent top contact and the doped substrate controls the excitonic energy as well as the recombination and spin lifetime of the carriers. The out-of-plane electron spin polarization is obtained from the different intensity of the right (I_R) and (I_L) circular components of the photoluminescence emitted when electrons and holes recombine.

3. EXPERIMENTAL DETAILS

The experimental studies were carried out in a single GaAs quantum well (SQW) with a thickness of 25 nm, embedded within $Al_xGa_{1-x}As$ layers in the intrinsic region of a n-i-p diode structure grown along the [111]B direction, cf. Fig. 2 (a detailed description of the sample growth conditions can be found in Ref. [1]). The bias voltage, V_b, applied between the top n-doped layer and the p-doped substrate generates the vertical electric field E_Z necessary for BIA/SIA-compensation. In order to laterally confine the electric field region in the surface (x-y), the top n-doped layer and part of the top (Al,Ga)As spacer within the intrinsic region were chemically etched into mesa structures with a diameter of 300 µm.

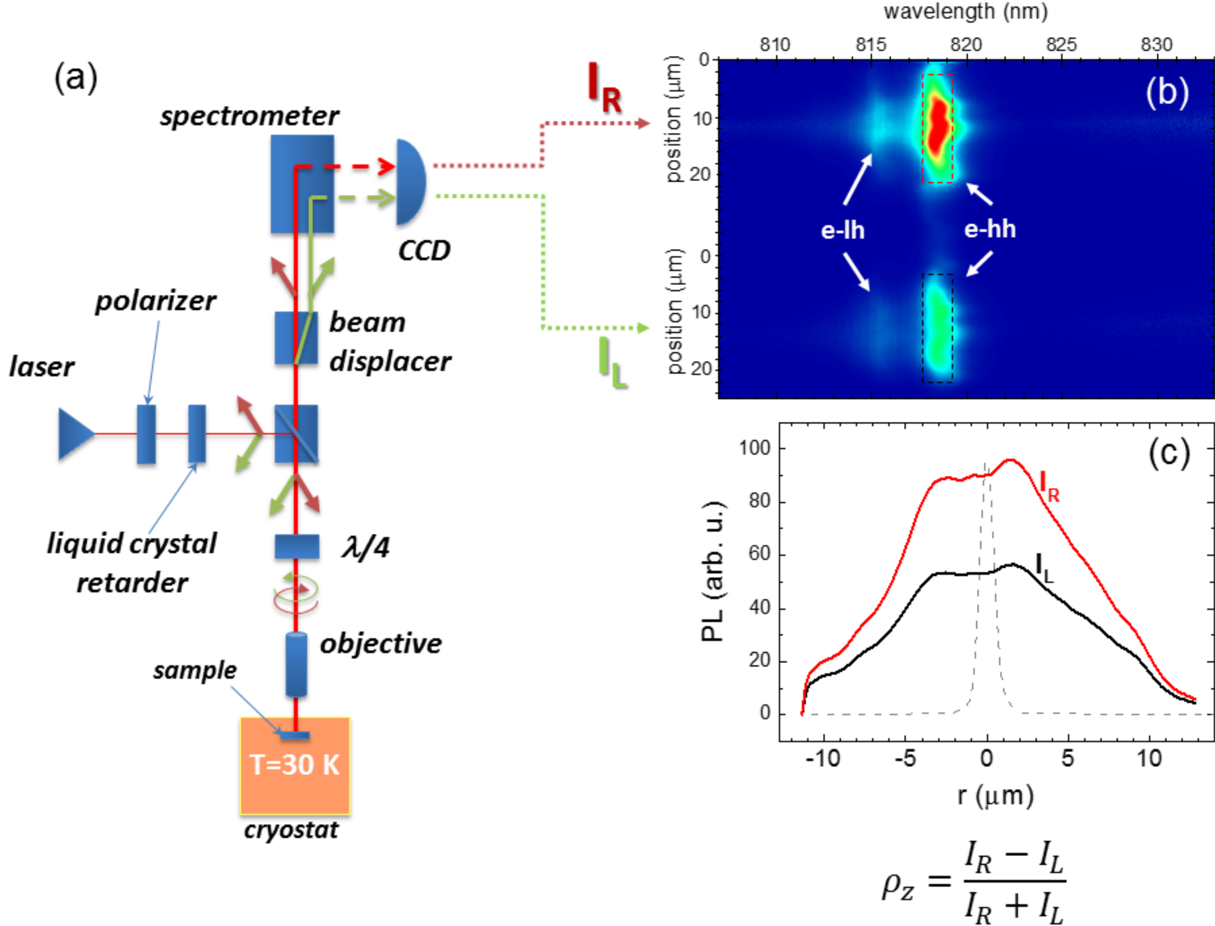

Figure 3 (a) Setup for the optical detection of spin transport using polarization-resolved photoluminescence (PL). The sample is hold at low temperatures (approx. 30 K) in an optical cryostat. Out-of-plane spin-polarized carriers are excited by a circularly polarized laser beam from a tunable Ti:Sapphire laser. The input laser polarization is defined by the liquid crystal retarder and a λ/4 plate placed on the beam path. The laser is focused on a spot with a diameter of 1.5 µm on the sample surface using a microscope objective. The PL emitted from the region around the excitation spot is collected by the same objective and focused on the input slit of an optical spectrometer. The λ/4 plate and the beam displacement prism on the detection path direct the right (I_R) and left (I_L) circular PL components to different positions along the input slit. (b) PL image detected by a cooled charge-coupled detector (CCD) at the spectrometer output. The image shows the PL components I_R and I_L with spectral (horizontal scale of the PL image) and position sensitivity (vertical scale). *e-hh* and *e-lh* denote the spectral features associated with electron-light hole and electron-heavy hole transitions. (c) Corresponding intensity profiles for I_R and I_L obtained by integrating the PL signal in the image in (b). The gray line displays, for comparison, the spatial dependence of the reflectivity of the tightly focused laser beam employed for PL excitation, from which we determine the spatial resolution of the setup. The optical technique thus allows the simultaneous detection of the spatial distribution of the carrier density and spin polarization. Time-resolved profiles can be obtained by using a pulsed laser synchronized with a gated CCD camera.

For the polarization-resolved optical experiments, the samples were placed in a cold-finger optical microscope cryostat with electric connections for the application of the electric bias. The estimated measurement temperature is 30 K. The experimental procedure employed to probe the spin dynamics and detect spin transport is depicted in Fig. 3. The spins were optically excited using a circularly polarized 756 nm pulsed laser beam tightly focused onto a spot with a diameter of 1.5 μm (full width at half maximum, FWHM), time-averaged flux of 20 μW, and a repetition rate of 25 MHz. The photoluminescence (PL) emitted around the excitation spot was detected with spatial and time resolution using the approach described in Fig. 3, which yields profiles for PL from electron-heavy hole transitions with left (I_L) and right (I_R) circularly polarization for different delay times after laser excitation. The latter were obtained by synchronizing a time-gated charge-coupled device detector (CCD, gate time of 500 ps) with the trigger of the laser pulses. Figure 3(b) shows a PL image obtained by the CCD detector with the spatial dependence of the PL for right and left circular polarization around the excitation spot. Figure 3(c) displays the corresponding PL intensity profiles, which indicate a clear excess of right circularly polarized photons. Note, in particular, that the excited spin polarized carriers spread and emit over a region much larger than the diameter of the excitation spot (determined by the reflection profile of the laser beam, grey dashed curve). The PL profiles were then used to determine the spin polarization according to $\rho_Z=(I_R-I_L)/(I_R+I_L)$. As the spin polarization of the holes is lost in a few picoseconds, the difference between I_L and I_R gives information about the out-of-plane spin polarization of the electron ensemble.

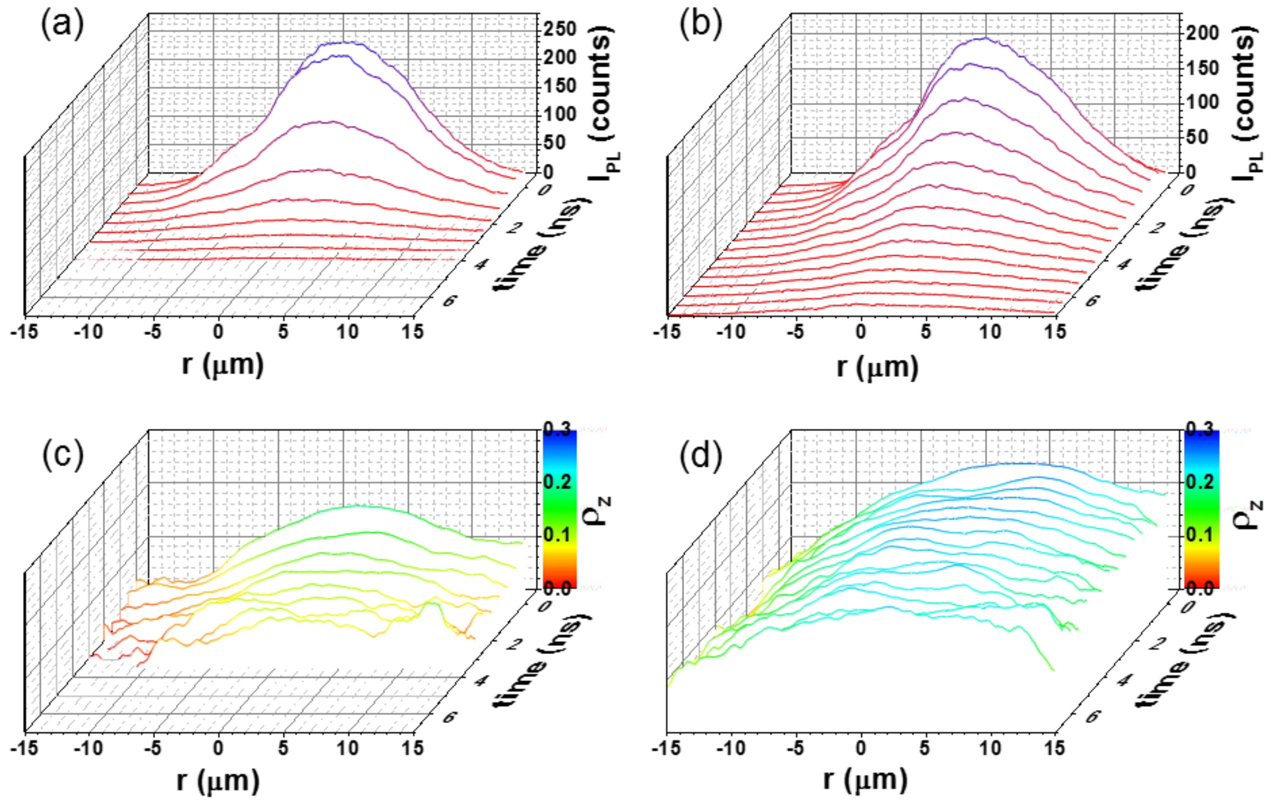

Figure 4. Spatial distribution of the PL intensity, I_{PL}, measured using the technique described in Fig. 3 under biases (a) V_b=0 and (b) V_b=-1.5 V as a function of the time delay after the laser pulse. Panels (c) and (d) show the spatial distribution of the out-of-plane spin polarization, ρ_Z, recorded under the same conditions as (a) and (b), respectively.

4. RESULTS

Figure 4(a) and 4(b) compare spatial PL profiles (corresponding to the average PL intensity $I_{PL}=I_L+I_R$) recorded under reverse biases V_b=0 and -1.5 V, respectively, after different time delays following laser excitation. In both cases, the emission region extends to distances *r* much larger than the dimensions of the excitation spot (with a diameter of 1.5 µm, cf. Fig. 3(c)). The latter is attributed to the radial transport of the photo-excited carriers driven by thermal diffusion as well as by repulsive forces active just after the laser pulse (delay times below 500 ps). These forces arise from the repulsive interaction between the excitons (and possibly also free carriers) at the high density regions close to the generation spot. For V_b=0, the carrier recombination lifetime is 0.8 ns, so that after 2.5 ns all carriers have already recombined and the diameter of the emission region (corresponding to the full width at half maximum of the spatial profiles) is limited to approx. 10 µm. At reverse biases around E_C (cf. Fig. 4(b)), the electric field E_Z reduces the spatial overlap between the electron and hole wave functions via the quantum confined Stark effect. As a result, both the recombination lifetime (2.4 ns) and the spatial extension of the emission region increase considerably (the FWHM of the profiles reaches 20 µm after 6 ns).

The large widths of the PL profiles allow us to determine the spin polarization at radial positions much larger that the size of the laser excitation spot. Figure 4(c) and 4(d) display the spin polarization profiles corresponding to those of Figs. 4(a) and 4(b), respectively. Note that the spin polarization is maintained for transport distances comparable to the width of the PL profiles (i.e., for distances from the generation area exceeding 10 µm).

A further important point is that both the decay time and the decay length of the out-of-plane spin polarization, ρ_Z, can be controlled by the applied bias (cf. Figs. 4(c) and 4(d)). Whereas for V_b=0 the value of ρ_Z after 2 ns is already less that 0.1, in the case of Vb=-1.5 V the out-of-plane spin polarization is still above 0.2 over the full extension of the spin ensemble after 6 ns delay.

In order to obtain information about the mechanisms governing this behavior, we compare in Fig. 5 the time decay profiles for I_{PL} and ρ_Z determined from Fig. 4 at the origin ($r = 0$). The PL lifetime increases monotonically with increasing reverse bias $|V_b|$ (cf. Fig. 5(a)). The decay time for ρ_Z, in contrast, initially increases for $|V_b|<1.8$ V, where it reaches a maximum, and then decreases for larger $|V_b|$, as illustrated in Figs. 5(b) and 5(c). Note that spin lifetimes approaching 50 ns are obtained for $|V_b|$=1.8 V.

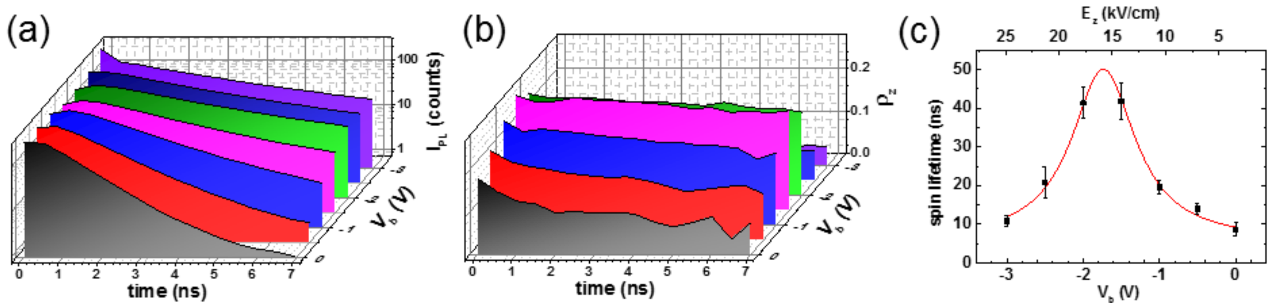

Figure 5: Time-resolved profiles for the (a) PL intensity, I_{PL}, and (b) out-of-plane spin polarization, ρ_Z, recorded at the origin (i.e., r=0). The profiles were extracted from those of Fig. 4. (c) Dependence of the spin lifetime on applied bias V_b (lower horizontal scale) and the corresponding electric field E_Z (upper horizontal scale). The maximum spin lifetime corresponds to the point where the Rashba field compensates the Dresselhaus one (i.e., $E_Z=E_C$, cf. Eq. 1). The red line is a guide to the eye.

5. DISCUSSIONS AND CONCLUSIONS

As discussed in Secs. 1 and 2, an electric field applied perpendicular to the QW plane enhances the spin lifetime via two mechanisms: (i) the reduction of electron-hole exchange scattering due to the reduced overlap between the electron and hole wave functions, and (ii) the reduction of spin decoherence when the total SO-field reaches a minimum due to the

compensation of the Rashba and Dresselhaus contributions. While mechanism (i) may play a significant role at low reverse bias (i.e., for fields lower than the compensation field E_C given by Eq. 1), it cannot account for the maximum in the bias dependence displayed in Fig. 5(c). The observation of a maximum in Fig. 5(c) unambiguously establishes the BIA/SIA compensation as the mechanism for bias-induced spin lifetime enhancement in (111) QWs. The values for the compensation field $E_C \approx 16$ kV/cm determined in the spatially resolved measurements presented in the previous section also agree very well with those obtained using a large laser spot (cf. Ref.[1,4]).

In addition to the spin lifetime enhancement, the results of the previous section give clear experimental evidence for the transport of spin coherence in (111) QWs. While a bias-induced enhancement of the spin lifetime in (111) QWs (as in Fig. 5(c)) has been reported in the literature [4, 7], spatially-resolved experiments required to access the spin transport have so far not been carried out for these structures. The demonstration of spin transport as well as of the bias dependence of the transport efficiency reported here are novel and qualitatively different from previous investigations of the spin dynamics in (111) structures.

In conclusion, we have shown that the application of vertical electric fields enables the efficient suppression of the SO-interaction in GaAs (111) QWs at low temperatures, thus increasing the spin lifetime and allowing the transport of spins over microscopic distances (>10 μm) comparable to the width of the PL profiles. The combination of spatially and time-resolved PL measurements presented here allows the access to spin transport dynamics in these structures and to determine the dependence of the transport distance on the applied electric field. The favorable properties of (111) GaAs QWs makes them an excellent platform for furthers studies of the spin dynamics as well as for spintronics applications.

ACKNOWLEDGMENTS

We thank Dr. Lopes for a discussion as well as M. Höricke, S. Rauwerdink, and A. Tahraoui for MBE growth and sample processing. We gratefully acknowledge financial support from the German DFG (priority program No. SSP1285).

REFERENCES

[1] A. Hernández-Mínguez, K. Biermann, R. Hey, and P. V. Santos, Phys. Status Solidi B **in print**, (2013).
[2] B. A. Bernevig, J. Orenstein, and S.-C. Zhang, Phys. Rev. Lett. **97**, 236601 (2006).
[3] J. D. Koralek et al., Nature **458**, 610 (2009).
[4] A. Hernández-Mínguez, K. Biermann, R. Hey, and P. Santos, Phys. Rev. Lett. **109**, 266602 (2012).
[5] X. Cartoixa, D. Z.-Y. Ting, and Y.-C. Chang, Phys. Rev. B **71**, 045313 (2005).
[6] I. Vurgaftman and J. R. Meyer, J. Appl. Phys. **97**, 053707 (2005).
[7] A. Balocchi et al., Phys. Rev. Lett. **107**, 136604 (2011).
[8] K. Biermann, A. Hernández-Mínguez, R. Hey, and P. V. Santos, J. Appl. Phys. **112**, 083913 (2012).